X-ray and birefringence orientation measurements on uniaxially deformed polyethylene film

Richard J. Pazur, Abdellah Ajji and Robert E. Prud'homme*
Centre de Recherche en Sciences et Ingénierie des Macromolécules, Département de Chimie, Université Laval, Québec, Canada G1K 7P4
(Received 30 September 1992; revised 5 February 1993)

Characterization of the crystalline and amorphous orientation of a uniaxially deformed low-density polyethylene (LDPE) film has been accomplished by combining pole figure X-ray diffraction and birefringence measurements. Characterization of the crystalline regions of the extruded film reveals the existence of a row-nucleated morphology with the *a* axis preferentially oriented in the plane containing the machine (MD) and transverse (TD) directions and the *b* axis strongly oriented along the film normal. This morphology is embedded in an amorphous matrix, biaxially oriented in nature. Low uniaxial extension along the MD produces two major orientational states in the crystalline regions which seem independent of the corresponding amorphous orientation. The pole figure analysis clearly shows that the *c* axis weakly orients towards the MD. Upon further uniaxial extension, it begins to tilt progressively away from the stretching direction inducing a complementary orientational behaviour between the *c* and *b* crystallographic axes on account of the stationary *a*-axis orientation perpendicular to the stretching direction. At higher draw ratios, the *c* axis gradually realigns itself with the stretching direction and uniaxial orientational states in all regions of the microstructure are obtained, indicating the existence of a fibrillar-type morphology. Quantification of the induced orientation was carried out and compared in terms of Hermans, Nomura/Kawai and White/Spruiell orientation functions.

(Keywords: polyethylene; orientation; deformation)

INTRODUCTION

The uniaxial deformation of semicrystalline polymers causes enormous organizational changes in their microstructure. It is generally agreed that the deformation takes place by slip, twinning and through martensitic transformations[1]. But it is evident that the deformation modes arising upon elongation are contingent upon the initial morphology of the sample. Molecular orientation measurements assist in understanding the deformation processes operating in the microstructure and allow one to follow the evolution of these changes with elongation. On the basis of such measurements it may be possible to infer a deformation model for a given specimen. Uniaxial elongation progressively aligns the molecular chain axes along the stretching direction which consequently increases tensile properties such as Young's modulus. Therefore, the need to characterize the type and magnitude of molecular orientation in deformed polymer systems is imperative if one wishes to comprehend the deformation processes induced and to optimize properties.

The uniaxial bulk deformation behaviour of row-nucleated structures, typically found in extruded polyethylene (PE) films, have generally received little investigation. This lamellar-stacked morphology can exist in two extreme orientational forms and/or combinations thereof, depending upon the amount of stress present during crystallization in the bulk[2]. Under low stress conditions, the lamellae grow epitaxially about the oriented fibrous rows and twist periodically and symmetrically around the *b* crystallographic axis. This crystallization process causes a preferential orientation of the *a* axis along the stress direction, parallel with the lines of nucleation. Higher stress in the melt causes the lamellae to crystallize regularly without twisting, causing the *c* axis to become oriented along the stress direction.

The uniaxial deformation behaviour of PE possessing a *c*-axis orientation has been investigated using dynamic orientation measurements by Suehiro *et al.*[3]. Their results suggest that the deformation of this morphology takes place primarily in two steps: (1) initial rotation of the crystallites about the crystal *b* axis, consequently causing the *c* axis to orient further towards the stretching direction; and (2) bending of the lamellae between tie-links reminiscent of a leaf-spring, as suggested by the constant *b*-axis orientation. This second mode of deformation requires the existence of highly localized tie molecule bridges between adjacent lamellae[4].

Brady and Thomas[5] have recently proposed a deformation model of a *c*-axis oriented row-nucleated morphology in terms of decrystallization, the step-wise mechanical reduction and reorganization of the crystalline phase. By transmission electron microscopy, they observed the initial formation of craze-like cavities in the non-crystalline regions, akin to the leaf-spring

* To whom correspondence should be addressed

0032-3861/93/194004-11

behaviour explained earlier. Further elongation in the stressed phase incited the appearance of the monoclinic unit cell in association with (1 0 0)⟨0 0 1⟩ and (0 1 0)⟨0 0 1⟩ crystal shear, which in due course causes a reduction in crystal size. Decrystallization inevitably produces a fibrillar-type morphology at high elongations.

Concerning the orientational processes occurring during the uniaxial deformation of an *a*-axis row-nucleated morphology, Aggarwal *et al.*[6] have shown, using X-ray diffraction techniques, that the deformation of a PE film restretched along the machine direction (MD) passes by an initial step where the preferential *a*-axis orientation is replaced by a random orientation of the crystallites. Further deformation takes place as in unoriented PE (as summarized by Keller[7]), which begins by the perpendicular orientation of the *a* axis, followed by the inclination of the *c* axis about the stretching direction, which subsequently aligns itself along this direction at high draw ratios.

In the present study, the uniaxial deformation behaviour of a row-nucleated low-density polyethylene (LDPE) film will be investigated. The magnitude of the crystalline and amorphous orientation will be determined by combining X-ray pole figure and birefringence measurements. Quantification of the experimental results will lead to the characterization of the induced orientation by Hermans, Nomura/Kawai and White/Spruiell orientation functions. A critical examination of the effectiveness of these latter functions to characterize molecular orientation will also be carried out.

REPRESENTATION OF MOLECULAR ORIENTATION

The orientation distribution of a structural unit, whose position is specified with respect to Cartesian coordinates by Euler-type angles can be represented mathematically by a series of orthogonal functions (see review in ref. 8). If the discussion is limited to the determination of the orientation of the r_jth vector of the distribution, which is placed at the origin of the structural unit and to the second moment of the orientation distribution, it is possible to simplify the initial Euler-angle-based equations to the following[9]:

$$F^j_{20} = (3\langle\cos^2\phi_{jz}\rangle - 1)/2 \quad (1)$$

and

$$F^j_{22}/3 = \langle\cos^2\phi_{jx}\rangle - \langle\cos^2\phi_{jy}\rangle \quad (2)$$

where the angles ϕ_{jk}, describing the position of the r_jth vector with respect to each Cartesian axis k, are defined as in *Figure 1*. The angular brackets signify an average value of the functions. Measurements of orientation in this fashion, originally proposed by Wilchinsky[10], satisfy the condition:

$$\sum_k \langle\cos^2\phi_{jk}\rangle = 1 \quad (3)$$

Equation (1), perhaps better known as the Hermans orientation function, specifies an average orientation of the vector r_j with respect to the reference axis z in terms of the angle ϕ_{jz}, and thus is used to characterize uniaxial orientational states. Alone, it takes on the following values depending upon the orientation state being characterized: $F^j_{20} = 0$ (no orientation present, isotropic system), 1 (perfect uniaxial orientation), or -0.5 (perpendicular orientation). Equation (2), hereafter called the Nomura/Kawai second moment orientation function, has the following limiting values: $F^j_{22}/3 = 0$ (isotropic system or uniaxial orientation along z), 1 (uniaxial orientation along x), or -1 (uniaxial orientation along y). This function can characterize not only a uniaxial orientation along z, but also those along the x or y axes.

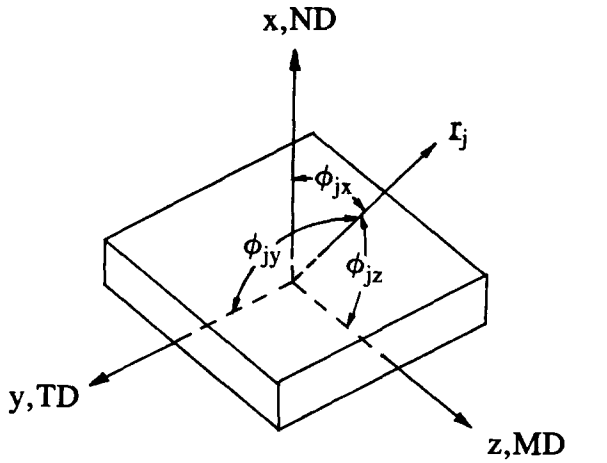

Figure 1 The orientation of the r_jth vector defined by the angles ϕ_{jk} in the Cartesian coordinate system. The reference directions of the polymer specimen may also be represented in terms of extruded film notation (MD = machine direction, TD = transverse direction and ND = normal direction). These two notations are used interchangeably in this study

The orientation functions presented up to this point assume that the system possesses only one symmetry axis, which is commonly defined as the fibre axis. To this end, interpretation of uniaxial orientational states is straightforward. However, characterization of biaxial orientational states remains unclear. With this in mind, White and Spruiell developed biaxial orientation functions which depend upon the symmetry of the polymer specimen[11]. Fibres have one reference axis, whereas polymer films conventionally have two, which are defined as the two axes contained within the film plane, z and y. As well as deriving the Hermans orientation function for uniaxial orientation, they also developed biaxial orientation functions with respect to the z and y axes, which have the following form:

$$F^B_{zj} = 2\langle\cos^2\phi_{jz}\rangle + \langle\cos^2\phi_{jy}\rangle - 1 \quad (4a)$$

$$F^B_{yj} = 2\langle\cos^2\phi_{jy}\rangle + \langle\cos^2\phi_{jz}\rangle - 1 \quad (4b)$$

where B refers to biaxial orientation states. The following orientational states can be characterized by the use of this function: (1) $F^B_{zj} = 1$ and $F^B_{yj} = 0$ (uniaxial orientation along z); (2) $F^B_{zj} = 0$ and $F^B_{yj} = 1$ (uniaxial orientation along y); (3) $F^B_{zj} = -1$ and $F^B_{yj} = -1$ (uniaxial orientation along x); or (4) $F^B_{zj} = 1/2$ and $F^B_{yj} = 1/2$ (equal planar biaxial orientation). Equal biaxial orientation states satisfy the following equation:

$$\langle\cos^2\phi_{jz}\rangle = \langle\cos^2\phi_{jy}\rangle = (1 - \langle\cos^2\phi_{jx}\rangle)/2 \quad (5)$$

which also describes equal planar orientations when $\langle\cos^2\phi_{jx}\rangle = 0$.

It is possible to plot the biaxial orientation functions, F^B_{zj} and F^B_{yj}, in the form of an isosceles triangle (*Figure 2*). The apices of this triangle describe perfect uniaxial orientational states with respect to the x, y and z reference axes, while the altitude indicates equal biaxial

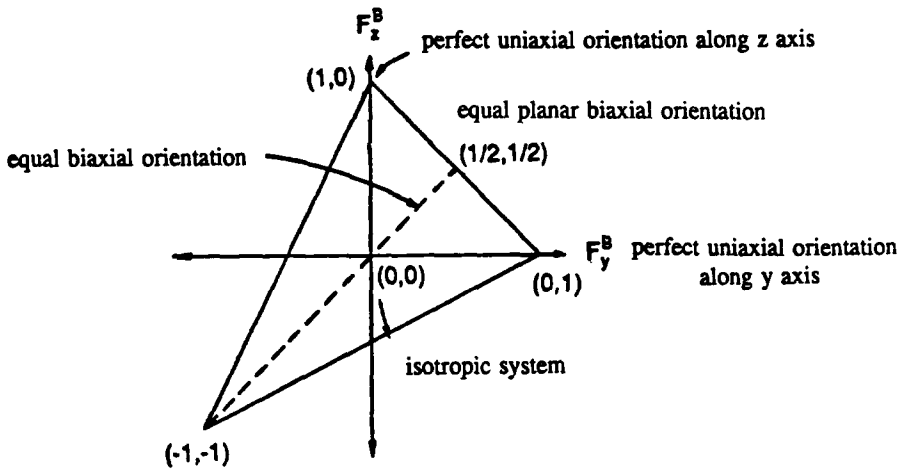

Figure 2 The White/Spruiell orientation triangle plotted according to the values of F_z^B and F_y^B calculated by equation (4)

orientational states according to equation (5). Planar-type orientation is represented along the base of the triangle, and zero orientation (isotropic systems) by the origin. These biaxial orientation functions have already been applied to PE to characterize orientation in blown film[12,13] and blow-moulded bottles[14].

Birefringence

The birefringence Δ_{ij} is defined as the difference in refractive index between the orthogonal directions i and j. In Cartesian coordinates, where three reference directions are assigned to the specimen (*Figure 1*), one can define three birefringences:

$$\Delta_{zx} = n_z - n_x \tag{6a}$$

$$\Delta_{zy} = n_z - n_y \tag{6b}$$

$$\Delta_{yx} = n_y - n_x \tag{6c}$$

It is necessary to relate the birefringences calculated by equations (6) to the orientational state of the system. In an isotropic system, the three birefringence values are nil. In systems presenting a uniaxial orientation along z, and thus a cylindrical symmetry, the following birefringence values are observed:

$$\Delta_{zy} = \Delta_{zx} \text{ and } \Delta_{yx} = 0 \tag{7}$$

For polymer films, an equal deformation along the z and y axes would produce a biaxially oriented system with[13]:

$$\Delta_{zx} = \Delta_{yx} > \Delta_{zy} \tag{8}$$

Upon calculating the birefringence and applying equations (7) and (8), it is possible to differentiate between uniaxial and biaxial orientations in polymer systems.

X-ray diffraction

Probably the best and most exploited technique for measuring crystalline orientation in polymer systems is X-ray diffraction. Pole figures offer many advantages over traditional photographic techniques. By means of a stereographic projection, the three-dimensional orientation of a diffraction plane is displayed on a planar map consisting of contour intensity lines. The precise location, as well as the intensity of the orientation, of a molecular plane distribution with respect to the three reference directions may both be observed on the pole figure. Moreover, it can be used to distinguish visually between different orientational states of a system (i.e. uniaxial and biaxial). For a given crystalline plane (*hkl*), the evaluation of $\langle \cos^2 \phi_{hkl,z} \rangle$ with respect to the reference axis z can be carried out by the following equations[15]:

$$\langle \cos^2 \phi_{hkl,z} \rangle = \frac{\int_0^{\pi/2} I(\phi) \sin \phi \cos^2 \phi \, d\phi}{\int_0^{\pi/2} I(\phi) \sin \phi \, d\phi} \tag{9a}$$

$$I(\phi) = \int_0^{2\pi} I(\phi, \beta) \, d\beta \tag{9b}$$

The normal to a family of crystalline planes (*hkl*) is represented by vector r_j of *Figure 1*. The sum of the average squared cosine terms with respect to each reference axis k satisfies equation (3). Once all the values of $\langle \cos^2 {}_{hkl,k} \rangle$ have been obtained, it is possible to evaluate and then compare the values obtained from the orientation functions introduced in the preceding section.

In this study of PE film, we will assume the simple two-phase model of a polymer[16]. In this case, it is possible to write the birefringence in terms of the crystallinity X, intrinsic birefringences Δ_i^o and orientation functions by form of the following equation:

$$\Delta_{ij} = X\Delta_c^o f_c + (1-X)\Delta_{am}^o f_{am} + \Delta_f \tag{10}$$

where Δ_f is the form birefringence and the subscripts c and am refer to the crystalline and amorphous phases, respectively. This equation is useful for determining the amorphous orientation f_{am} in systems possessing uniaxial orientation. For characterizing biaxial orientation, White and Spruiell have incorporated their orientation functions into equation (10) with the result that:

$$\Delta_{zx} = X(F_{zc}^{Bc}\Delta_{cb}^{oc} + F_{za}^{Bc}\Delta_{ab}^{oc}) + (1-X)\Delta_{am}^o F_z^{Ba} + \Delta_f \tag{11a}$$

$$\Delta_{yx} = X(F_{yc}^{Bc}\Delta_{cb}^{oc} + F_{ya}^{Bc}\Delta_{ab}^{oc}) + (1-X)\Delta_{am}^o F_y^{Ba} + \Delta_f \tag{11b}$$

where Δ_{cb}^{oc} and Δ_{ab}^{oc} are the intrinsic birefringences of the cb and ab planes of the orthorhombic crystal lattice, F_{zc}^{Bc}, F_{yc}^{Bc}, F_{za}^{Bc}, F_{ya}^{Bc} are the biaxial orientation functions of the c and a axes, and F_z^{Ba} and F_y^{Ba} represent amorphous orientation functions.

EXPERIMENTAL

The orientation of a commercially prepared flat film of LDPE has been studied. Deformation of the LDPE film was carried out on an Instron tester (model 1130). Rectangular-shaped samples of dimensions 12 cm by 3.5 cm were cut with the long axis along the MD. These samples were stretched at 25°C at a rate of 0.5 cm min^{-1}, to particular draw ratios $\lambda_{initial}$ and then, upon release of the applied load, immediately allowed to relax to final draw ratios λ. This experimental procedure prevented the appearance of necking and permitted an array of draw ratios up to the rupture point of the samples to be obtained easily.

The densities, d, of the initial and re-oriented films were determined at room temperature by using an isopropyl alcohol–diethylene glycol gradient density column having a density range between 0.90 and 1.00 g cm^{-3}. The degree of crystallinity, X, was calculated by:

$$X = \frac{d_c(d - d_{am})}{d(d_c - d_{am})} \tag{12}$$

where, for PE[17], $d_c = 1.00$ g cm^{-3} and $d_{am} = 0.855$ g cm^{-3}.

The three birefringences Δ_{ij} of equation (6) were calculated by measuring the refractive indices of the oriented films with an Abbé refractometer (Bausch and Lomb, model 3L), fitted with a Polaroid, using a mixture ($n_D^{25} \approx 1.54$) of α-chloronaphthalene (Anachemia) and silicon oil (Union Carbide R-850)[18]. In this study, the experimental error of Δ_{ij} was found not to exceed 0.0005.

Pole figures of the diffraction planes of PE were obtained using a Rigaku X-ray machine (Rotaflex RU-200 BH). This apparatus consists of a rotating anode (6000 rev min^{-1}), a scintillation counter coupled with a pulse-height analyser and a goniometer upon which is placed the semi-automatic pole figure assembly (Rigaku, model B-8). All X-ray measurements were carried out with nickel-filtered CuKα radiation of wavelength 0.154187 nm produced at 55 kV and 190 mA. The software (Rigaku, D/MAX-B) calculates the second-order orientation function obeying equation (3) with respect to the machine (MD), transverse (TD) and normal (ND) reference directions of the sample, and also plots the pole figures. All pole figures were subjected to a nine-point smoothing process incorporated in the software. Two experimental techniques are required to measure the intensities of equation (9) at a given Bragg angle θ, for angles α between 0° and 90° (note that $\alpha = 90° - \phi$) and β between 0° and 360° of the pole figure. The Decker transmission technique was used for $0° \leqslant \alpha \leqslant 75° - \theta$ while the Schultz reflection method, which requires a Schultz slit, was used to complete the interior of the pole figure for values of α up to 90°. Widths of the receiving and scattering slits required for the two experimental techniques were determined by the procedure outlined in the Rigaku manual (ME200DL8), and varied between 2 and 6 mm depending upon the sample and the Bragg angle investigated. An angle step of 5° for α and β was employed during the measurements. Correlation of the two techniques was carried out by standardizing the intensities for three common values of α. Experimental background intensities were measured above and below the Bragg angle investigated except for the (2 0 0) plane, where one measure was taken at higher 2θ in order to avoid the strong diffraction overlap from the (1 1 0) plane. For a typical diffraction peak, both background intensities were averaged over all angles β for each given α and, subsequently, subtracted from each experimental intensity. Absorption effects during transmission and reflection have also been corrected[15].

PE belongs to the orthorhombic crystal system and its lattice constants are well known (a = 7.417, b = 4.945 and c = 2.547). Its molecular chain axis is defined parallel to the c crystallographic axis. Desper and Stein[19] have shown for systems possessing an orthorhombic unit cell that:

$$\sum_{j=a,b,c} \langle \cos^2 \phi_{jk} \rangle = 1 \tag{13}$$

for each reference direction k. The direct measurement of the orientation of the chain axis of PE via the (0 0 2) plane is possible for studying uniaxial orientation[20]. However, in order to study more complex forms of orientation, i.e. double or biaxial, it is advantageous to know not only the orientation of the chain axis, but also that of the unit cell. The exact orientation of the PE unit cell can be resolved by including measurements of the (2 0 0) and (0 2 0) planes.

RESULTS AND DISCUSSION

Rectangular strips of the LDPE film cut along the MD were stretched to draw ratios of $\lambda_{initial}$ and then allowed to relax completely to values of λ. A waiting time of approximately 1 month assured the stability of the microstructure and, therefore, the consistency of the drawn film properties[21]. *Figure 3* presents $\lambda_{initial}$ as a function of λ. For low initial draw ratios, relaxation effects dominate as $\lambda_{initial} \approx \lambda$. Beyond $\lambda_{initial} = 2.5$, however, a linear relationship is observed between $\lambda_{initial}$ and λ, indicating a permanent deformation. As an example, uniaxial restretching of the LDPE film along the MD up to $\lambda_{initial} = 3.0$ produces, after total relaxation, a sample of $\lambda = 1.59$. All reported draw ratios λ and orientation calculations hereafter presented will refer to residual stress values.

The birefringence values of the initial and restretched films were calculated from the measured refractive indices by equation (6) and plotted *versus* draw ratio in *Figure 4*. The initial film is weakly anisotropic in nature as it possesses birefringences of $\Delta_{zx} = 0.0015$, $\Delta_{zy} = 0.0019$ and

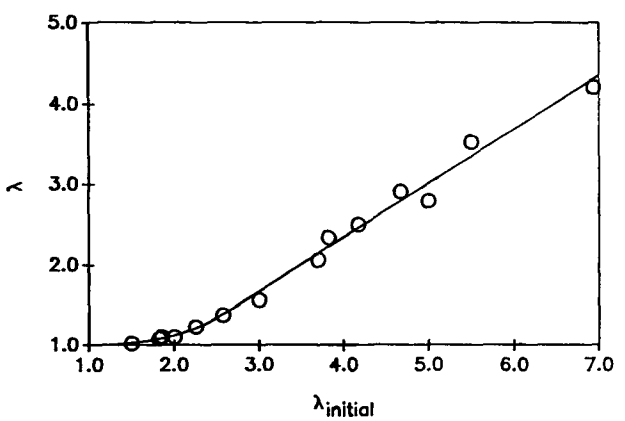

Figure 3 Uniaxially oriented samples of LDPE were prepared by stretching along the MD to draw ratios $\lambda_{initial}$. The samples contracted upon relaxation to final draw ratio values λ

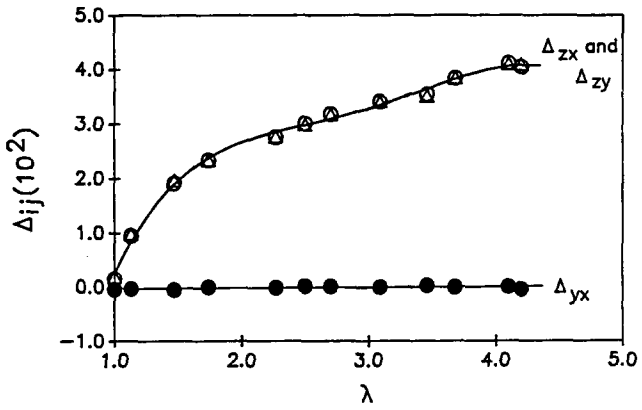

Figure 4 Evolution of uniaxial orientation in LDPE with respect to draw ratio presented in terms of birefringence

$\Delta_{yx} = 0.0004$. These values satisfy, within experimental error, equation (7) and thus suggest an initial global uniaxial orientation of the film along its MD. Upon restretching along the MD, the birefringences Δ_{zx} and Δ_{zy} increase rapidly at low draw ratios and gradually level off to a maximum value of 0.041 before the breaking point of the films. The birefringence Δ_{yx} is effectively nil throughout the whole range of draw ratios investigated. These birefringence curves, characteristic of a semicrystalline polymer undergoing uniaxial extension, obey equation (7) and thus indicate the presence of uniaxial orientation in the system for all draw ratios. These results agree with those of Schael[22] who also measured the three birefringences by a refractometer in order to quantitatively characterize the orientation in restretched PE films.

Pole figures of the (2 0 0), (0 2 0) and (0 0 2) planes were constructed for the initial and restretched films as a function of draw ratio and are presented in *Figure 5*. At first glance it is apparent that the *a* axis is preferentially aligned in the MD/TD plane with, however, a slight tendency to orient along MD. (Note that diffraction from the (1 1 0) crystalline plane did not affect appreciably the intensity distribution collected for the (2 0 0) plane[23].) Perhaps more striking than the planar *a*-axis orientation is the strong *b*-axis orientation normal to the plane of the film, as shown by the (0 2 0) pole figure. Diffraction from the (0 0 2) plane was weak, as noted by the unsymmetrical form of its pole figure. In spite of this anomaly, it is still possible to infer that the *c* axis of the film is randomly oriented about the perimeter of the MD/TD plane. In summary, the initial extruded film possesses a strong *b*-axis orientation normal to the film plane, which consequently causes the *a* and *c* axes to lie within this plane. Furthermore, the *a* and *c* axes are oriented radially in this same plane. This type of molecular orientation has been observed in highly blown LDPE film, but only by the (2 0 0) and (0 2 0) pole figures[24]. It is most likely that this film contains an *a*-oriented row-nucleated morphology which is more or less evenly distributed between the MD and TD of the film. Since the *b* axis is the lamellar growth direction of PE, preferential nucleation at the film surface would cause a strong *b*-axis orientation along ND.

From *Figure 5* it is seen that re-orientation of the crystalline regions does not take place uniaxially for all draw ratios, contrary to the conclusion drawn from the birefringence results. The initial planar *a*-axis orientation has separated into four maxima in the MD/TD plane: two follow the MD and two are located approximately 31° from the TD (*Figure 5.2*). It is peculiar that the orientation is unsymmetrical in nature as it appears only in the second and fourth quadrants of the pole figure. The *b*-axis orientation remains strongly aligned along the ND, but starts to spread out in the ND/TD plane. However, the most striking result is the appearance of broad maxima at the MD poles for the (0 0 2) plane, indicating that there is a tendency for the chain axis to orient along this direction. Interpretation of the initial three pole figures upon restretching suggests that the unit cell has taken on at least two preferred orientations. One population of crystals has the *a* axis aligned predominantly along the MD. The second population of crystals seems to have the *c* axis oriented along the MD, the *b* axis along the ND and the *a* axis aligned with the TD poles. Some rotation exists about the *b* axis (±35°), which gives some freedom of movement to the *a* and *c* axes in the MD/TD plane. The significance of this second preferred orientational population is uncertain, but could be related to possible recrystallization owing to the sample preparation method[25]. It is clear that a further pole figure analysis for $1.0 < \lambda < 1.04$ would be helpful in deducing the deformational processes that have taken place.

As λ is increased to a value of 1.12 (*Figure 5.3*), the prior *a*-axis orientation along the MD ($\lambda = 1.04$) is completely removed, as it now becomes more or less randomly oriented in the ND/TD plane of the sample. The change in orientation for the (2 0 0) plane, which takes place from $\lambda = 1.04$ to $\lambda = 1.12$, is quite remarkable and has been commonly observed in PE deformation studies. Upon studying the pole figure for the (0 2 0) plane at $\lambda = 1.12$, it is evident that a rotation in its orientation of approximately 35°, confined to the second and fourth quadrants of its pole figure, has taken place about the ND axis. The magnitude of its change in orientation is much less in comparison to the (2 0 0) plane. It is well known for PE that the orientation of the *a* axis is much more efficient than that of the *b* axis for small deformations. The *c* axis orientation begins to broaden about the MD. Because of the unique symmetrical state emerging, which involves an inclination of the *c* axis with respect to the MD, it is much more convenient to describe its orientation by the angle ϕ_{cz} of *Figure 1* rather than the pole figure angles α and β. The *c* axis is inclined to the MD at an angle ϕ_{cz} of 28°. But this initial inclination is confined in the MD/TD plane of the specimen and is observed only in the first and third quadrants. This special inclination of the *c* axis seems to coincide, within error, to the 35° rotation of the orientation band of the *b* axis and suggests the emergence of a unique orientation population. In this case, it seems that the unit cell has adopted an orientation in which the *a* axis is fixed along the ND, forcing the *b* and *c* axes in the MD/TD plane at their well-defined angles of inclination. The *b* axis seems to have some liberty to turn about the *c* axis and, hence, is not always confined to the MD/TD plane. The primary orientational population, which was seen emerging at $\lambda = 1.04$, has the *b* axis aligned along the ND, the *c* axis along the MD, and the *a* axis oriented preferentially along the TD.

At $\lambda = 1.25$, little change is noticed in the orientation of the *a* axis as it remains strongly aligned in the ND/TD plane (*Figure 5.4*). On the other hand, the (0 2 0) pole figure for this draw ratio now contains two series of bands

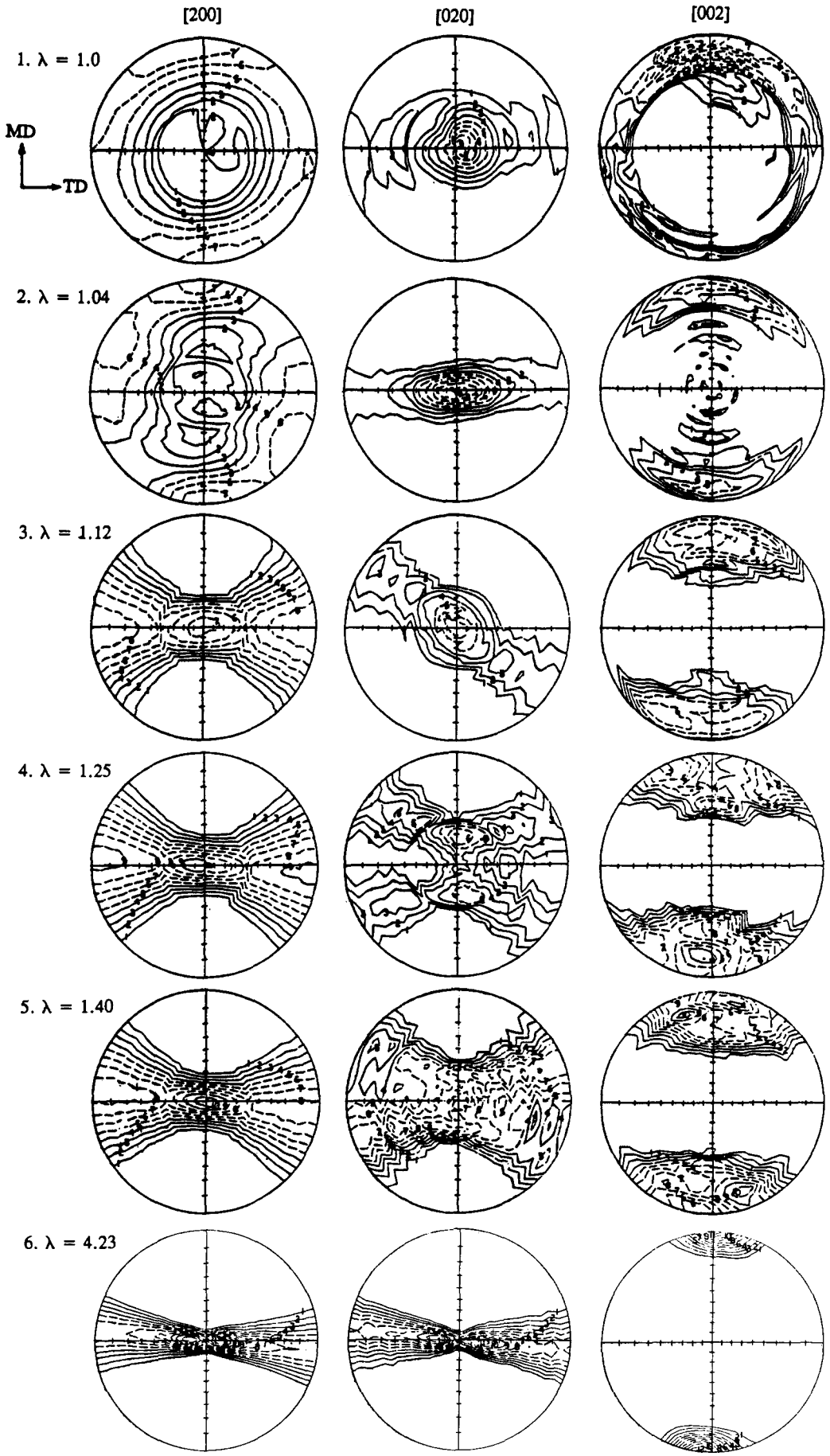

Figure 5 Pole figures of the (2 0 0), (0 2 0) and (0 0 2) planes of: (1) the extruded LDPE film, and the restretched films to λ values of (2) 1.04; (3) 1.12; (4) 1.25; (5) 1.40; (6) 4.23

of high orientation, symmetric about each MD pole for $51° \leqslant \phi_{bz} \leqslant 64°$. The bands of high orientation criss-cross the pole figure in a manner reminiscent of the seams of a baseball. The *c* axis has continued to broaden around the MD, shifting the maximum orientation away from the MD poles to ϕ_{cz} values varying between 25 and 36°. Contrary to its orientational behaviour at $\lambda = 1.12$, inclination of the *c* axis is complete for all angles about the MD. (Note that the variation observed in the values of ϕ_{bz} and ϕ_{cz} could be due to the improper alignment of the MD of the specimen with respect to the pole figure sample holder for $\alpha = 0°$ and $\beta = 0°$ and/or to earlier restretching not exactly along the MD.) It is evident that only the *b* and *c* axes are experiencing re-orientation because the form of the *a*-axis orientation has remained stationary during these draw ratios ($\lambda = 1.12$ and 1.25). This suggests the creation of a unique orientational state composed of one orientational population which is different from the transitional states observed earlier at $\lambda = 1.04$ and $\lambda = 1.12$. The inclination of the *c* axis with respect to the drawing direction is expected upon uniaxial deformation of isotropic PE, as it has been seen[26] to topple to values of $\phi_{cz} = 35°$. We believe that the direct observation of this phenomenon by use of the (0 0 2) pole figure has not been reported elsewhere.

For $\lambda = 1.40$, the *a*-axis orientation is unchanged in the ND/TD plane (*Figure 5.5*) while the *b* and *c* axes continue to re-orient themselves. It is hard to depict a difference in the *b*-axis orientation, but it seems that the two bands of orientation are beginning to coalesce in the middle of the pole figure in the ND/TD plane. This is confirmed by the values of ϕ_{bz} which have increased to values between 57 and 69°. Orientation of the *b* axis is becoming more pronounced along the TD. The band of high orientation of the *c* axis is beginning to converge upon the MD poles as ϕ_{cz} decreases in value.

For much higher draw ratios ($\lambda = 4.23$), pole figures representative of a uniaxial system are obtained (*Figure 5.6*). The *a* and *b* axes are randomly oriented in the ND/TD plane as the *c* axis is aligned along the MD. Since the *a*, *b* and *c* axes are mutually perpendicular, the three pole figures clearly depict the existence of a cylindrical symmetry and, hence, uniaxial orientation.

The complementary orientational behaviour of the *b* and *c* axes, described by the angles ϕ_{bz} and ϕ_{cz} respectively, has been plotted as a function of draw ratio in *Figure 6*. Since the *a* axis is preferentially oriented in the ND/TD plane during this phenomenon, the sum of ϕ_{bz} and ϕ_{cz} is restricted to 90°. The complementary orientational behaviour seems to start for draw ratios beyond $\lambda = 1.12$ (i.e. after the initial orientational transition period) and quickly peaks for draw ratios before $\lambda = 1.25$. In our study, the average values of ϕ_{cz} and ϕ_{bz} reached maxima graphically at approximately 31 and 57°, respectively. For all draw ratios thereafter, a gradual diminution of the complementary orientation is observed. Completion of this orientational behaviour was estimated by extrapolation and should occur for draw ratios of 2.5. It is likely that the transition from the complementary orientation of the *b* and *c* axes to a true uniaxial orientation of the *c* axis at $\lambda = 2.5$ is synonymous with the appearance of a fibrillar-type morphology in the redrawn films.

Values of $\langle \cos^2 \phi_{jk} \rangle$ were evaluated by equation (9) for the initial and uniaxially restretched films. *Table 1* summarizes the experimental data acquired on the initial

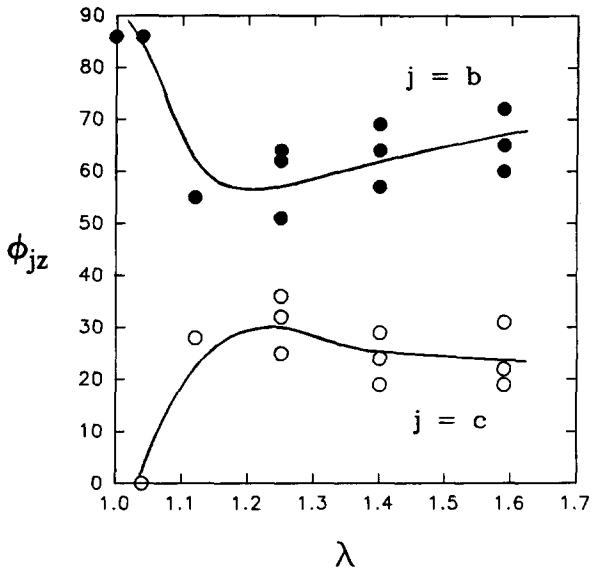

Figure 6 The complementary orientational behaviour of the *b* and *c* axes illustrated as a function of draw ratio. ϕ_{jz} values were taken, where possible, from the perimeter of the pole figure ($\alpha = 0°$) and as the α value for $\beta = 0°$

Table 1 Values of $\langle \cos^2 \phi_{jk} \rangle$ were computed from the (2 0 0), (0 2 0) and (0 0 2) pole figures of the LDPE film. Values of $\langle \cos^2 \phi_{ck} \rangle$ were evaluated assuming the exactness of $\langle \cos^2 \phi_{ak} \rangle$ and $\langle \cos^2 \phi_{bk} \rangle$

Film	*k*	$\langle \cos^2 \phi_{ak} \rangle$	$\langle \cos^2 \phi_{bk} \rangle$	$\langle \cos^2 \phi_{ck} \rangle$	$\langle \cos^2 \phi_{ck} \rangle$
LDPE	MD	0.376	0.272	0.397	0.352
	TD	0.374	0.328	0.358	0.298
	ND	0.260	0.405	0.255	0.335

film. The first three columns of averaged squared cosines were evaluated directly from the corrected intensities obtained from the (2 0 0), (0 2 0) and (0 0 2) pole figures of *Figure 5.1*. The last column represents $\langle \cos^2 \phi_{ck} \rangle$ values calculated strictly by equation (13) using the experimental values of $\langle \cos^2 \phi_{ak} \rangle$ and $\langle \cos^2 \phi_{bk} \rangle$. One observes that the sum of any $\langle \cos^2 \phi_{jk} \rangle$ over the three reference directions *k* for a given *j* gives approximately unity and hence fulfils the requirements of equation (3). Evaluation of equation (13) by use of the experimental values of the averaged squared cosine gives roughly unity, but with a slightly larger error of about 10%. Since the diffraction intensities measured from the (0 0 2) plane were generally weak, we have decided to evaluate the values of $\langle \cos^2 \phi_{ck} \rangle$ by using equation (13) and the values of $\langle \cos^2 \phi_{ak} \rangle$ and $\langle \cos^2 \phi_{bk} \rangle$. Diffraction measurements on a thin film (thickness 144 μm) reduce the precision of the experimental $\langle \cos^2 \phi_{ck} \rangle$ values. Moreover, there is the possibility of some interference[20] from the (5 2 0) plane, which diffracts at the same Bragg angle as (0 0 2).

The Hermans and Nomura/Kawai crystalline orientation functions were calculated by equations (1) and (2) with respect to the MD and then conveniently plotted on the same graph as a function of draw ratio (*Figure 7*). For the initial film ($\lambda = 1.0$), the following values of these functions were evaluated: $F^c_{az} = 0.064$, $F^c_{bz} = -0.092$, $F^c_{cz} = 0.028$ and $F^a_{22}/3 = -0.114$, $F^b_{22}/3 = 0.077$ and $F^c_{22}/3 = 0.037$. The values of F^c_{az} and F^c_{bz} of the Hermans function reveal a weak uniaxial orientation of the *a* axis

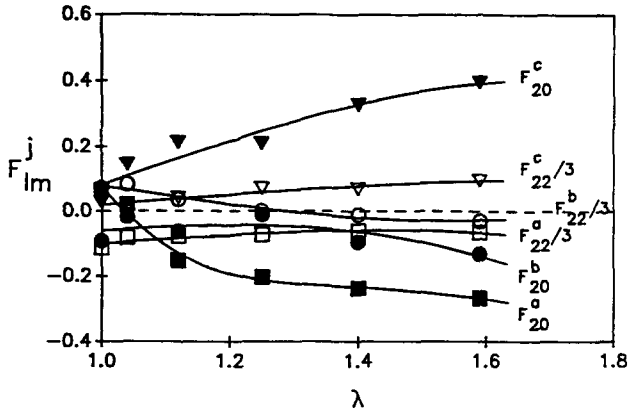

Figure 7 Hermans and Nomura/Kawai orientation functions were calculated for each j crystallographic axis with respect to the MD, and plotted as a function of λ

along the MD with the b axis perpendicular to the MD. The c axis is weakly oriented given its near-zero value of F^c_{cz}. The negative values of $F^a_{22}/3$ infer that the a axis is also oriented along the TD. The perpendicular orientation of the b axis is mostly concentrated along the ND on account of the positive values of $F^b_{22}/3$. Interpretation of $F^c_{22}/3$ seems to be difficult, but on the basis of the orientational behaviour of the a and b axes, the c axis cannot be uniaxially oriented along the MD. The near-zero values of $F^c_{22}/3$ suggest that the c axis is randomly distributed and, by deduction, confined to the MD/TD plane of the sample. Use of these two functions together is imperative if a good interpretation of the orientation is desired. It is also apparent that the interpretation of the orientation function values can be quite difficult without recourse to the corresponding pole figures. Upon restretching, F^c_{20}, representing the orientation of the c axis, generally increases with draw ratio, indicating the progressive alignment of the chain axis along the machine stretching direction. The curve for F^b_{20} shows a maximum of roughly zero when $\lambda = 1.25$, which coincides with the climax of the complementary orientational state. The curve for F^a_{20} decreases in value for all draw ratios, indicating that a perpendicular orientation of the a axis has been induced. Indeed, to have a true uniaxial orientation state at low draw ratios, the shape of the F^a_{20} and F^b_{20} curves should be similar, which is of course not the case for this study. Siesler[27] has reported the same behaviour of the Hermans orientation function for uniaxially deformed PE by using Fourier transform infra-red spectroscopy. The Nomura/Kawai orientation function for each crystalline axis varies little with draw ratio and remains close to zero. By definition of this function, and given that the drawn system is not isotropic, one can only conclude that a uniaxial orientation state is produced along the MD with increasing draw ratio. However, in this case, this function is not sensitive to the complementary orientational behaviour observed between the b and c axes.

Characterization of the orientation in the initial and restretched films was also carried out by evaluating White/Spruiell biaxial orientation functions by equation (4). These results are presented graphically in *Figure 8*. This figure suggests a biaxial crystalline character of the initial film. The orientational states of its three crystallographic axes are in the proximity of the biaxial orientation line. The a axis is in fact biaxially oriented in the MD/TD plane of the film as its initial orientation function values fall directly upon the dashed line. Evolution of the orientational states induced upon restretching to λ values can be conveniently followed on this diagram by means of the arrows. It is observed that the value of F^B_{za} becomes rapidly negative with increasing draw ratio, indicating perpendicular orientation of the a axis to the stretching direction, with an almost equal distribution of orientation between the ND and TD. F^B_{zb} and F^B_{yb}, however, both increase in value and approach the equal biaxial orientation line for draw ratios up to 1.25. Given the form of its pole figure at $\lambda = 1.25$ (*Figure 5.4*), the b axis is neither randomly oriented nor biaxially oriented as deduced from the diagram, but symmetrically oriented in bands about the MD. This particular type of orientation cannot be deduced wholly from the biaxial orientation function. Values of F^B_{zc} increase with draw ratio and diminish slightly at $\lambda = 1.25$ when values of F^B_{yc} are negative. Beyond λ values of 1.25, F^B_{zc} increases at the expense of F^B_{zb}, indicating the beginning of a normal uniaxial-type orientation behaviour of the c and b axes. F^B_{zc} tends towards unity for higher draw ratios.

The crystalline and amorphous orientation functions were evaluated by using equation (10) and then plotted as a function of draw ratio in *Figure 9*. In this equation, we have assumed zero contribution of the form birefringence, $\Delta^o_c f_c = 0.0286(3\langle\cos^2\phi_{cz}\rangle - 1)$ for uniaxially stretched PE[28] and $\Delta^o_{am} = 0.058$ as verified in ref. 29. The crystalline birefringence equation assumes a cylindrical symmetry of the orientation during uniaxial stretching. A density of 0.915 g cm^{-3} was measured for the initial LDPE film and was used to evaluate X by equation (12). It was impossible to observe a difference between the measured density values in the restretched samples and hence the degree of crystallinity was considered constant for all draw ratios. In the initial film, the magnitude of crystalline and amorphous orientation is similar. However, upon weak deformation ($1.0 < \lambda < 1.2$), the crystalline regions are observed to orient faster than the amorphous ones. This phenomenon has been reported elsewhere for restretched PE[30]. It is likely that the amorphous regions relax faster than the crystallites, thus producing this initial discrepancy. For higher draw ratios, a similar orientational behaviour is observed in both regions. For the specimen of $\lambda = 4.23$, $f_c = 0.733$ and

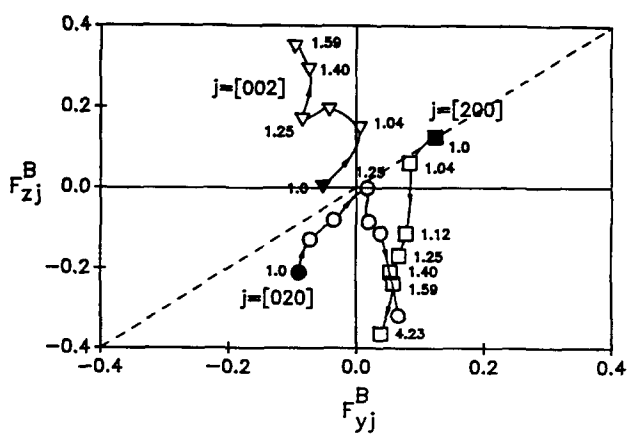

Figure 8 Evolution of the orientation experienced by the uniaxially stretched LDPE samples as a function of draw ratio, presented on a White/Spruiell orientation triangle

$f_{am}=0.702$. These results tend to agree with those of Stein and Norris[28] in that f_c is generally greater than f_{am} at high elongations in restretched PE film.

The White/Spruiell amorphous orientation functions were evaluated by equation (11) and then plotted along with the c axis biaxial crystalline orientation functions as a function of draw ratio in *Figure 10*. The magnitude of amorphous orientation is comparable with that of the crystalline orientation throughout the whole stretching range. For the initial film, $F_z^{Ba}=0.053$ and $F_y^{Ba}=0.038$, which suggest by their similarity in magnitude that a certain amount of biaxial orientation is present in the amorphous regions. For $\lambda=1.04$, this orientation diminishes as F_y^{Ba} approaches zero, possibly signifiying the onset of a uniaxial orientational state. For higher draw ratios, F_z^{Ba} increases proportionately with λ as F_y^{Ba} remains stable and oscillates between values of 0.038 and 0.081. Despite the non-zero values of F_y^{Ba}, it is possible to conclude that the orientational behaviour of the amorphous regions is predominantly uniaxial. For $\lambda=4.23$, $F_z^{Ba}=0.724$ and $F_y^{Ba}=0.085$ which indicates the predominance of F_z^{Ba} over F_y^{Ba} for higher draw ratios. It is possible that the relaxation of the stretched samples causes the non-zero values of F_y^{Ba}. We also note the similarities between the F_z^{Ba} and F_{zc}^{B} curves of *Figure 10* with f_{am} and f_c of *Figure 9*. Despite some differences in magnitude for the orientation functions, the curves show the same orientation behaviour in the crystalline and amorphous regions. The added advantage of the biaxial orientation functions is that a uniaxial orientation is not postulated and that values of F_{yj}^{B} may be compared with the F_{zj}^{B} values.

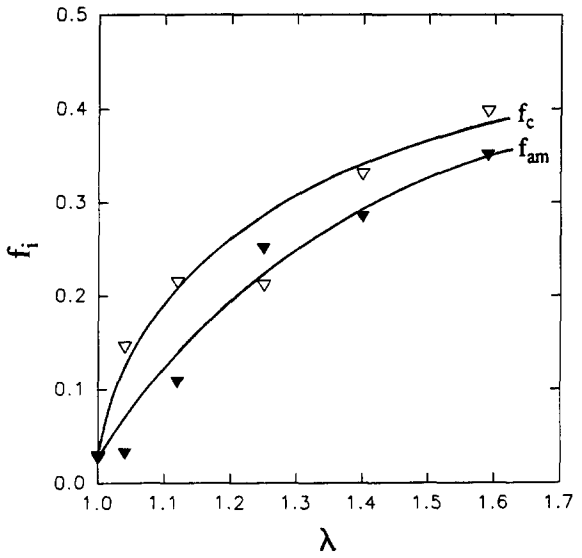

Figure 9 Plot of the uniaxial crystalline and amorphous orientation functions as a function of draw ratio

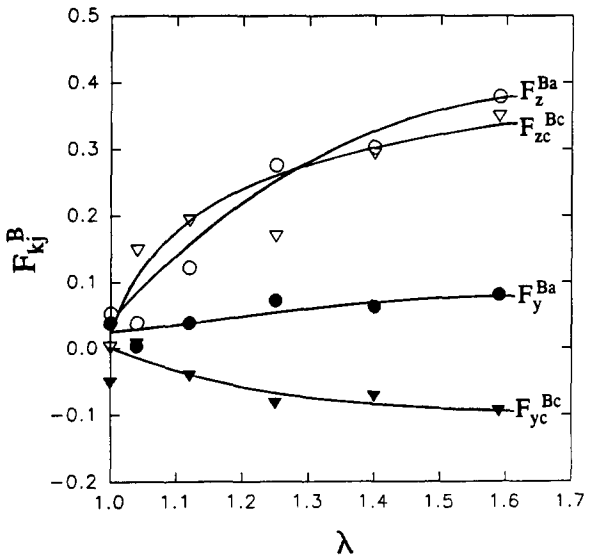

Figure 10 Plot of the White/Spruiell biaxial orientation functions for the crystalline and amorphous regions as a function of draw ratio

Table 2 summarizes the orientational states observed in the various phases of the LDPE film as a function of draw ratio. Restretching of the film causes enormous morphological changes in the crystalline regions, because of the complex orientational states produced therein. These orientational states should correspond to the destruction of an a-axis oriented row structure which is oriented in the MD/TD plane. This seems to take place orientation-wise in three major steps. The initial planar orientation of the a axis is progressively destroyed upon restretching, being replaced by an orientational state in which the a and c axes have switched positions by rotation about the b axis. It seems that, once all the initial planar a-axis orientation has been transformed into this weak c-axis orientational state along the MD, the emergence of another transitional state involving the inclination of the c axis with respect to the MD becomes favourable. The very onset of this orientational state has the c axis confined to the MD/TD plane, with its inclination forcing the b axis out of the MD/TD plane. Further deformation invokes the true development of this orientational state, as the c axis begins to wobble freely about the MD entailing the same complementary behaviour of the b axis. The a axis remains oriented in the ND/TD plane during the complementary orientational phase. It is necessary to point out that the exact transition

Table 2 Summary of the types of orientation observed in the crystalline, amorphous and crystalline/amorphous regions together during the restretching of a LDPE film along its MD

Structure characterized	$\lambda=1.0$, initial film	$1.0<\lambda\leqslant 1.12$	$1.12<\lambda\leqslant 2.5$	$\lambda>2.5$
Crystalline	a-Axis orientation along MD/TD	c-Axis orientation along MD	Complementary orientation of b/c axes	Uniaxial orientation
Amorphous	Weakly biaxial		Uniaxial orientation	
Crystalline + amorphous	Uniaxial orientation			

point between each of these orientational states is uncertain because two orientational populations were always observed in the small deformation region. The complementary orientational state seems to peak around $\lambda = 1.25$ for maximum tilting of the c and b axes, and then gradually diminishes upon restretching to values of $\lambda = 2.5$, where uniaxial orientation states begin to emerge. It is most probable that the transition between these two orientations is synonymous with a change in crystalline morphology; the heavily deformed row structure has at this point collapsed and is thereupon replaced by a fibrillar-type morphology. Except for high draw ratios ($\lambda > 2.0$), independent orientational behaviour is observed in the crystalline, amorphous and crystalline/amorphous regions as a unit. The amorphous regions remain biaxially oriented at low draw and begin to show uniaxial behaviour for draw ratios beyond $\lambda = 1.04$.

The crystalline orientational changes induced upon restretching generally agree with the earlier observation of Aggarwal *et al.*[6]. However, in our case we have observed the emergence of a weak c-axis orientational state along the MD after destruction of the planar a-axis orientation, contrary to their reported isotropic state. It is most likely, in their case, that relaxation enhanced the random orientation of the crystallites. In this study, residual orientation is present for small deformations. In fact, the initial orientational states are actually quite complex owing to the generation of orientation populations which can be clearly discerned by pole figures.

We note the substantial difference of the orientational behaviour between the a axis (this study) and the c-axis[3] oriented row-nucleated morphologies. In the latter case, the c axes of the unit cell in the initial morphology are already aligned with the MD, and hence deformation along the MD only increases the magnitude of molecular orientation. In the first case, however, not only is the magnitude of the orientation of the c axes changing but also the type of orientational state. The fact that different orientational processes are taking place in both cases suggests the existence of a unique deformation mechanism for both morphologies.

Characterization of the induced molecular orientation in systems possessing complex orientational states proves to be difficult upon sole use of orientation functions. The Hermans orientation function as defined will characterize only uniaxial states. Systems are considered isotropic by this function when complex orientational states are encountered. In fact, any deviation from normal uniaxial orientation should be considered as a cause for further investigation. One way to proceed in this case is to try the Nomura/Kawai orientation function. This function will give a further idea about the orientation of the crystallographic unit cell, but a complete characterization of the orientation will not be possible. If it is known that the system possesses complex orientational states, it would be wise to calculate immediately the White/Spruiell biaxial orientation functions. These functions, plotted on their corresponding isosceles triangle, will aid in the characterization of biaxial states, especially in the reference MD/TD plane of polymer films. Orientational representation in terms of a White/Spruiell diagram is practical, especially for following the evolution of orientation as a function of draw ratio. One orientational diagram can conveniently summarize the visual results given by a series of pole figures. But all conclusions derived by these orientation functions and their corresponding diagrams are contingent upon the pole figures from which they were calculated. The pole figure is the best method for conceiving the three-dimensional orientation of a crystalline plane. If one has access experimentally to the orientation of each crystallographic axis, one may thereupon deduce the orientation of the unit cell. Pole figures are useful for identifying the existence of different orientation populations of the unit cell in the system. However, the presence of orientation populations diminishes the effectiveness of quantification by orientation functions.

CONCLUSIONS

The characterization of the orientation induced upon mechanical uniaxial deformation of a LDPE film along its MD has been accomplished. Pole figure measurements indicated the presence of an a-axis orientation distributed radially in the MD/TD plane of the initial extruded film. The molecular chain orientation is confined to the same plane given the strong ND orientation of the b axis. This crystal orientation, typical of row-nucleated morphologies, is embedded in an amorphous matrix which is weakly biaxial in nature. For small deformations, independent orientation behaviour has been observed in the crystalline regions, in the amorphous regions and also in the crystalline/amorphous regions as a whole. The crystalline orientation behaviour is without doubt the most fascinating given the complicated orientational states produced therein. Upon restretching, at least three major orientational states develop in the crystalline regions:

1. rapid replacement of the planar a-axis orientation by a weak c-axis orientation along the MD;
2. development of a complementary orientational state between the b and c axes for reason of the stationary a-axis orientation; and
3. final collapse of the complementary orientational state which leads naturally to a true uniaxial orientational state possessing a cylindrical symmetry.

For small draw ratios ($\lambda \leqslant 1.04$), the amorphous regions remain biaxially oriented. However, at slightly higher elongations they slowly acquire a uniaxial orientation, as would be predicted by the pseudo-affine model for uniaxial deformations.

Hermans and Normura/Kawai orientation functions, useful together for characterizing uniaxial states of the crystallographic unit cell, were not sufficient to characterize the complex orientational states induced upon deformation. In our case, the White/Spruiell orientation functions provided more insight in discerning the type of orientation present, as they can characterize biaxial states with respect to the MD and TD of the film. Needless to say, all quantification by orientation functions was hindered by the presence of orientation populations which should be deconvoluted and analysed separately by the orientation functions. Complex orientation states can be most easily identified by a complete pole figure analysis.

ACKNOWLEDGEMENTS

This work was made possible through financial support from the Natural Sciences and Engineering Research

Council of Canada, and the Department of Education of the Province of Québec (Fonds FCAR and Action Structurante).

REFERENCES

1 Kinloch, A. J. and Young, R. J. 'Fracture Behaviour of Polymers', Applied Science Publishers, New York, 1983
2 Keller, A. and Machin, M. J. *J. Macromol. Sci. (Phys.)* 1967, **B1** (1), 41
3 Suehiro, S., Yamada, T., Kyu, T., Fujita, K., Hashimoto, T. and Kawai, H. *Polym. Eng. Sci.* 1979, **19**, 929
4 Peterlin, A. 'Structure and Properties of Oriented Polymers' (Ed. I. M. Ward), John Wiley, New York, 1975, Ch. 2
5 Brady, J. M. and Thomas, E. L. *J. Mater. Sci.* 1989, **24**, 3311
6 Aggarwal, S. L., Tilley, G. P. and Sweeting, O. J. *J. Polym. Sci.* 1961, **51**, 551
7 Keller, A. *J. Polym. Sci.* 1955, **15**, 31
8 Wolter, H. J., Vancso, G., Tomka, I. and Meissner, J. *Polym. Bull.* 1988, **19**, 389
9 Nomura, S. in 'Comprehensive Polymer Science' Vol. 2 (Eds G. Allen and J. C. Bevington), Pergamon Press, Toronto, 1989, p. 459
10 Wilchinsky, Z. W. *J. Appl. Phys.* 1959, **30**, 792
11 White, J. L. and Spruiell, J. E. *Polym. Eng. Sci.* 1981, **21** (13), 859
12 Ashizawa, H., Spruiell, J. E. and White, J. L. *Polym. Eng. Sci.* 1984, **24** (13), 1035
13 Choi, K. J., Spruiell, J. E. and White, J. L. *J. Polym. Sci., Polym. Phys. Edn* 1982, **20**, 27
14 Choi, K., Spruiell, J. E. and White, J. L. *Polym. Eng. Sci.* 1989, **29** (7), 463
15 Alexander, L. E. 'X-ray Diffraction Methods in Polymer Science', Wiley-Interscience, Toronto, 1969
16 Samuels, R. J. 'Structured Polymer Properties', John Wiley, Toronto, 1974
17 Brandrup, J. and Immergut, E. H. (Eds) 'Polymer Handbook' 3rd Edn, John Wiley, Toronto, 1989
18 Samuels, R. J. *J. Appl. Polym. Sci.* 1981, **26**, 1383
19 Desper, C. R. and Stein, R. S. *J. Appl. Phys.* 1966, **37** (11), 3990
20 Lafrance, C. P., Pézolet, M. and Prud'homme, R. E. *Macromolecules* 1991, **24**, 4948
21 Decandia, F., Vittoria, V. and Peterlin, A. *J. Polym. Sci., Polym. Phys. Edn* 1985, **23**, 1217
22 Schael, G. W. *J. Appl. Polym. Sci.* 1964, **8**, 2717
23 Pazur, R. J. MSc Thesis, Université Laval, Québec, Canada, 1990
24 Lindenmeyer, P. H. and Lustig, S. *J. Appl. Polym. Sci.* 1965, **9**, 227
25 Juska, T. and Harrison, I. R. *Polym. Eng. Sci.* 1982, **22**, 766
26 Krause, S. J. and Hosford, W. F. *J. Polym. Sci., Polym. Phys. Edn* 1989, **27**, 1853
27 Siesler, H. W. *Makromol. Chem.* 1989, **190**, 2653
28 Stein, R. S. and Norris, F. H. *J. Polym. Sci.* 1956, **21**, 381
29 Rossignol, J. M., Seguela, R., Rietsch, F. and Dupuis-Lallemand, J. *J. Polym. Sci., Polym. Lett. Edn* 1989, **27**, 527
30 Hoshimo, S., Powers, J., LeGrand, D. G., Kawai, H. and Stein, R. S. *J. Polym. Sci.* 1962, **58**, 185